NANO LETTERS

2004
Vol. 4, No. 5
921−926

The Significance of Plasma Heating in Carbon Nanotube and Nanofiber Growth

Kenneth B. K. Teo,[†] David B. Hash,[‡] Rodrigo G. Lacerda,[†] Nalin L. Rupesinghe,[†] Martin S. Bell,[†] Sharvari H. Dalal,[†] Deepak Bose,[‡] T. R. Govindan,[‡] Brett A. Cruden,[‡] Manish Chhowalla,[§] Gehan A. J. Amaratunga,[†] M. Meyyappan,[*,‡] and William I. Milne[†]

Department of Engineering, University of Cambridge, Cambridge CB2 1PZ, United Kingdom, Center for Nanotechnology, NASA Ames Research Center, Moffett Field, California 94035, and Department of Ceramics and Materials Engineering, Rutgers University, Piscataway, New Jersey 08854

Received March 6, 2004; Revised Manuscript Received March 26, 2004

ABSTRACT

The effect of the plasma on heating the growth substrate in plasma enhanced chemical vapor deposition (PECVD) of carbon nanotubes is characterized for the first time. This effect, which is commonly ignored in the nanotube/nanofiber literature, is the sole heating mechanism in this work for catalyst pretreatment and growth of straight and vertically aligned multiwalled carbon nanofibers. Significant temperatures, as high as 700 °C, are induced from a C_2H_2:NH_3 direct current (dc) plasma with no other heat source present. To model the behavior of the plasma-heated substrate platform, we have developed a 1-D dc discharge model that incorporates a cathode platform energy balance, including ion bombardment, thermal radiation, and solid and gas conduction. The predicted gas-phase species present are correlated with the morphology of nanofibers grown by exclusive plasma heating as well as by heating from plasma in combination with a conventional resistive heater. The understanding of plasma heating and its accurate modeling are essential for reactor design for wafer scale production of vertically aligned nanofibers.

Plasma enhanced chemical vapor deposition (PECVD) has been used widely now to produce multiwalled carbon nanotubes on patterned substrates. The resulting structures, as in the case of thermal CVD, appear to be predominantly curly, though the ensemble might look like vertical towers.[1] A more prominent and useful feature of PECVD is its ability to produce graphitized multiwalled carbon nanofibers that are indeed very straight, whisker-like, and vertically aligned. These can either be deposited in "forests" or as individual, free-standing structures.[1−4] Structurally, these are not completely hollow but have bamboo-like periodic closures along the stem, and hence are denoted simply as carbon nanofibers (CNFs) in this paper. The considerable interest in such nanofibers is due to their applications in electron-field emission,[5] nanoelectrodes,[6] filter media,[7] and as superhydrophobic surfaces.[8] A variety of plasma sources have been used in the production of the CNFs such as dc,[3,4] radio frequency (rf),[9] microwave,[10] and inductive plasma.[11] A summary of the efforts from various sources along with the current issues facing PECVD of carbon nanotubes/fibers can be found in ref 12.

* Corresponding author. E-mail: M.Meyyappan@nasa.gov.
† University of Cambridge.
‡ NASA Ames Research Center.
§ Rutgers University.

10.1021/nl049629g CCC: $27.50 © 2004 American Chemical Society
Published on Web 04/10/2004

One of the important issues in PECVD is the growth temperature, particularly, how low it can be maintained with the possibility to still obtain reasonable quality nanostructures. The general expectation from a plasma process is a growth temperature lower than that in thermal CVD for the same source gas since the plasma dissociates the feedstock more and a variety of carbon-bearing radicals and higher stable hydrocarbons become available for nanotube growth.[1,12] The surface reactions leading to nanotube growth from these plasma-produced species may proceed at lower temperatures with reasonable rates. Even if the rate-limiting step in growth is the carbon dissolution and diffusion into the metal particles, these rates are also dependent on temperature. Hence, substrate heating will impact both of these steps of the growth process. In addition to controlling the growth temperature, substrate heating plays a role in surface preparation, i.e., catalyst nanoparticle generation. This pretreatment step is highly specific to the nature of the catalyst, metal underlayer(s) if any, thickness of the catalyst, and the method used to deposit the catalyst on the substrate.

In most of the PECVD processes reported in the literature, an external heating source, mostly in the form of a resistance heater beneath the substrate-holding platform has been used.[1,3,4] In some cases, a hot filament hanging over the

substrate has been another source of heating.[2,13−15] In principle, a furnace or an IR lamp can also be the external source. In a PECVD process, the substrate is normally heated not only directly by the plasma but also due to this external source when used or activated. There have been only a few cases where an external substrate heater was not used,[16−18] and none of these cases obtained straight or well-aligned nanotubes. Recently, Boskovic et al.[19] claimed room temperature PECVD of curly nanofibers using an rf discharge; it is arguable whether the growth did proceed at room temperature since a relatively high power (200 W) was used and neither temperature measurement method nor substrate cooling was mentioned. In any case, the crystallinity (in terms of graphitization) is poor at lower temperatures as evident from published results[20] at 120 °C, which show short and conical structures rather than straight and whisker-like nanotubes/nanofibers. Note also that in ref 20 the plasma was assumed to have no effect on the substrate temperature. It is evident that plasma heating is not well recognized or understood by the nanotube community and is an issue that has to be addressed in detail.

A plasma can be an efficient source of heating the substrate. In a dc discharge, the power applied to the electrode is deposited into both the ions and electrons as they move through the sheath fields denoted by $\boldsymbol{J}\cdot\boldsymbol{E}$, where $\boldsymbol{J}$ is the current and $\boldsymbol{E}$ is the electric field. In this as well as other discharges using inductive, rf capacitive, and microwave plasma sources, these energized charged particles can then heat the gas in a plasma reactor through elastic collisions with electrons and charge exchange collisions with ions. The sample/substrate subsequently heats due to conduction from the hot gas as well as ion bombardment. Depending on process parameters such as power input and physical design, the substrate can reach temperatures as high as 700 °C for all types of plasma sources without the aid of an external heater. The purpose of the present work is to characterize the magnitude of this plasma heating and demonstrate that plasma heating alone is sufficient to pretreat a thin film to obtain catalytic nanoclusters and to grow straight and well-aligned nanofibers. The behavior of the plasma used for nanofiber synthesis and the mechanisms behind the plasma-induced heating are elucidated. The differences between nanofibers obtained through a plasma-heated process and nanofibers obtained from a combined plasma and tungsten wire-heated process are also examined.

The PECVD reactor used in this work has been described previously[4,21] and is capable of growing well-aligned and free-standing structures. The reactor consists of a suspended graphite cathode (exposed area 10 cm^2) and a gas showerhead of equal area 5 cm above it. The cathode is biased negatively with a dc power supply (Advanced Energy, MDX 1K). An electrically isolated thermocouple was embedded 1 mm into the graphite cathode to enhance its thermal contact for accurate temperature measurements. The graphite cathode also incorporates an embedded, rigid tungsten heater, enabling flexibility to resistively heat the substrate if desired in addition to the inherent plasma heating or by plasma heating only (with the resistive heater turned off). The resistance of the heater wires is only 0.1 ohm; therefore, whether the heater is turned on or off, the heating effect associated with the current flow through these wires due to the plasma power is negligible given that the maximum plasma current for this work is 0.3 A. Figure 1 shows photographs of the substrates when the plasma is the only heating source as well as the case with plasma and the external resistive heating; in both cases, the cathode is glowing red-hot at 700 °C. Note that in the case of Figure 1b, the plasma discharge solely was used to obtain this temperature. A 2-in. diameter Ta cathode in an independent reactor[15] was also observed to glow red-hot with plasma only at 200−300 W. While the extent of substrate heating itself depends on the plasma power and the thermal properties of the cathode and gas, it is clear from Figure 1b that deliberate cooling of the platform is necessary to obtain a low or room-temperature growth process since plasma heating is significant. The use of cooling has not been reported, except in ref 9 which uses an rf discharge in a confining magnetic field, without an external heater and with water-cooling of the electrode.

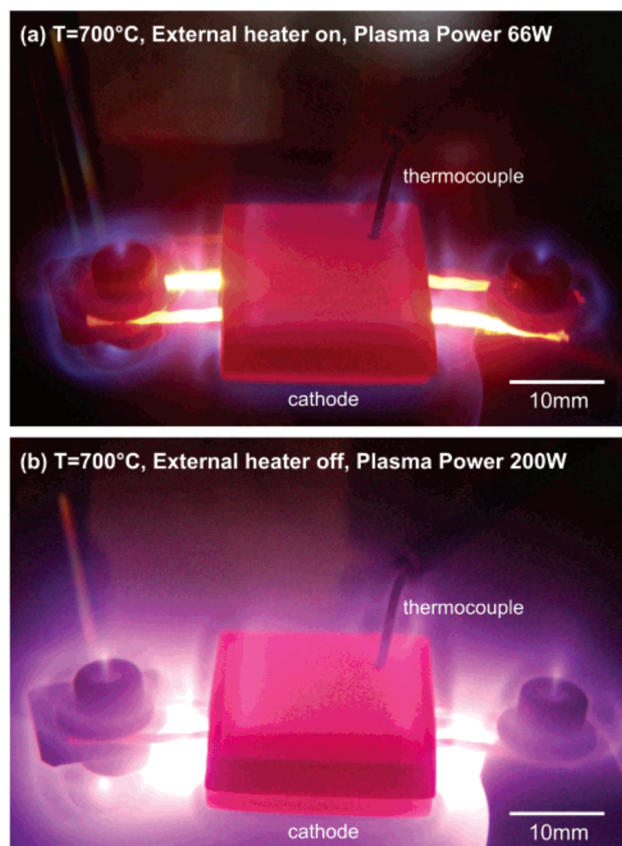

Figure 1. (a) Photograph (tilted side view) showing combined resistive heating using an external tungsten heater beneath the electrode and plasma heating (66 W dc power to the cathode) at 700 °C. (b) Plasma heating of the cathode at 700 °C, using 200 W of plasma power with the external heater off. The chamber was filled with a gas mixture of 54:200 sccm of C_2H_2/NH_3 at a pressure of 12 mbar. The thermocouple is mineral insulated with a stainless steel sheath and enters through the plasma (hot gas) zone before it is embedded in a 1−2 mm deep hole in the cathode.

Si⟨100⟩ substrates were coated with conductive indium tin oxide (15 nm thick) and Ni (7 nm) thin films by magnetron

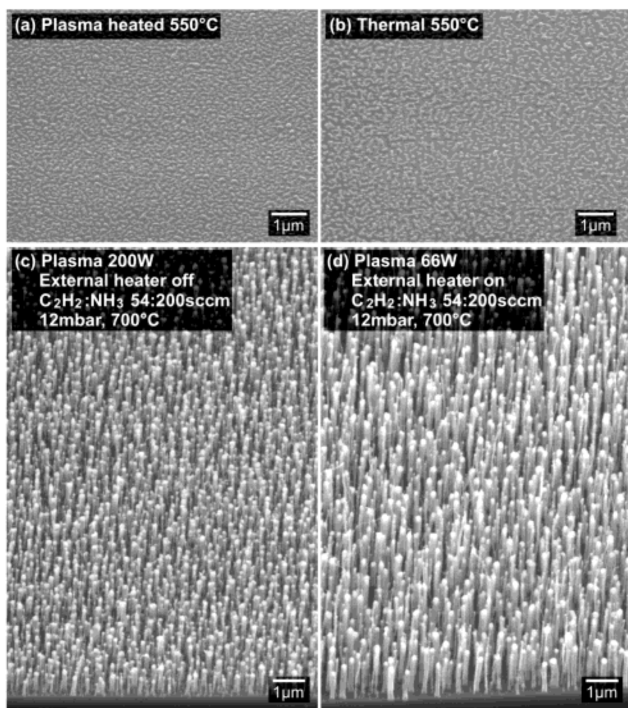

Figure 2. (a) Ni clusters formed from plasma heated cathode (120 W) in 200 sccm of NH_3, 12 mbar, 550 °C for 1 min. (b) Ni clusters formed from resistively heated cathode in 200 sccm of NH_3, 12 mbar, 550 °C for 1 min. (c) Nanofibers grown from plasma heating only (200 W plasma power, 54:200 sccm C_2H_2/NH_3, 12 mbar, 700 °C, 15 min). (d) Nanofibers from a "conventional" PECVD process (66 W plasma power in addition to external heating with the tungsten heater, 54:200 sccm C_2H_2/NH_3 12 mbar, 700 °C). The tilt was 45°.

sputtering. The catalyst thin film is usually treated by annealing at high temperature[4,10] or exposure to a hot filament[2,15] in a reducing atmosphere, and this causes the catalyst to transform into clusters which seed the nanofiber growth. Here, the substrate was placed on the cathode and a dc glow discharge was initiated at low power and low pressure (20 W, 2.5 mbar) in pure NH_3. The power and pressure were then simultaneously increased to 120 W and 12 mbar respectively, and a cathode temperature of 550 °C was typically obtained after just 1 min. This catalyst pretreatment procedure transformed the Ni thin film into nanoclusters as shown in Figure 2a. Note that these clusters are similar in morphology to nanoclusters obtained from thermal annealing of the same catalyst film under NH_3 at 550 °C for 1 min as shown in Figure 2b. After the NH_3 plasma-annealing step, C_2H_2 was introduced into the gas mixture and growth was performed at the desired plasma power without the aid of the tungsten external heater for 15 min. Figure 2c shows carbon nanofibers grown from such plasma heating only using 200 W of plasma power with gas mixtures of 54:200 sccm of C_2H_2/NH_3. The choice of 54:200 sccm of C_2H_2/NH_3 was based on previous studies[22] which showed that a gas mixture of ~20% C_2H_2/NH_3 was optimal for "clean" carbon nanofiber deposition, i.e., the substrate free of amorphous carbon. For comparison, Figure 2d also shows carbon nanofibers grown from the "conventional" PECVD process (i.e., one that uses inherent plasma heating and the external heater) using 54:200 sccm of C_2H_2/NH_3 and the catalyst preparation shown in Figure 2b; here the plasma power was adjusted to 66 W while tweaking the tungsten heater to achieve the same growth temperature of 700 °C as in Figure 5c. The obvious difference between the plasma-heated structures and the combined resistive/plasma heating process is that the latter structures are longer. These differences will be discussed later in the context of gas-phase composition.

The effect of plasma heating is now examined computationally by evaluating the substrate platform temperature as the plasma power is varied. A one-dimensional model previously reported for dc discharges[23] is extended to include an energy balance for the substrate platform. The complete model includes governing equations for the conservation of species mass, gas energy, ion energy, and electron energy, as well as equations to compute plasma potential and finally substrate temperature. Gas flow effects in the 1-D analysis have been included through a residence time source term in the mass and energy balance equations. A discussion of the specifics of these equations has been reported in earlier work.[23,24] The additional modeling of the substrate platform is implemented as a boundary condition to the gas energy equation

$$\sum_n \left(\kappa_s \cdot \nabla T + R_s D_s^T \cdot \nabla \ln \frac{P_s}{P} \right) - (1 - f) h_i J_i = \frac{\rho \overline{c'}}{4} \frac{2\alpha}{(2 - \alpha)} C_p (T - T_s) \quad (1)$$

with the following equations solved for the substrate temperature:

$$-f h_i J_i + \frac{\rho \overline{c'}}{4} \frac{2\alpha}{(2 - \alpha)} C_p (T - T_s) = \sigma \epsilon (T_s^4 - T_a^4) + h_c (T_s - T_a) \quad (2)$$

$$f = \frac{1}{1 + (E_i/a)^{-b}} \quad (3)$$

Expressing the boundary condition as the combination of eqs 1 and 2 allows for the modeling of the temperature jump at the cathode. If the pressure is high enough, the gas temperature T at the cathode will equal the cathode temperature T_s, and the solution will reduce to the sum of the two equations. The left-hand side of eq 1 is the gas heat flux at the cathode boundary and is comprised of thermal conduction, the Dufour heat flux, and the flux of reflected ion energy, respectively. Here, κ_s is the thermal conductivity, D_s^T is the thermal diffusion coefficient, R_s is the species gas constant, P_s is the species partial pressure, and the summation is over all neutral species. In eq 2, the terms on the left-hand side represent energy into the cathode, and those on the right represent energy out. The first term $f h_i J_i$ is the energy deposited by ion bombardment where h_i is the ion enthalpy, J_i is the ion flux, and f is the energy deposition coefficient

and is given by the empirical relation developed by Winters et al.[25] as shown in eq 3. The parameters a and b are empirically determined, and E_i is the ion energy. The second term on the left-hand side of eq 2 follows from the work of Leroy et al.[26] and models the heat flux from the gas where C_p is the gas specific heat at constant pressure, ρ is the gas density, and $\overline{c'}$ is the average thermal velocity. The thermal accommodation coefficient, α, represents the degree to which molecules incident on the cathode exchange energy with it. A value of 0.26 for all species with the exception of H_2 and H (0.17) was employed from data of thermal accommodation on graphite.[26]

The first term on the right-hand side of eq 2 represents heat loss due to thermal radiation of the graphite platform where σ is the Stefan−Boltzmann constant, ϵ is the graphite emissivity [$0.6924 + 0.0278$ (T/1000 K)], and T_a is the ambient temperature. The final term $h_c(T_s - T_a)$ represents the heat loss by conduction through the platform where h_c is the heat transfer coefficient of the platform apparatus. The heat transfer coefficient is generally written as a function of material thermal conductivity and thickness, $\kappa/\Delta x$; however, in the simulation, it is instead calibrated to the midpoint of the experimental data since the heat flow from the platform to ambient is much more complex than can be modeled by the simple expression, $\kappa/\Delta x$.

The parameters input for the simulations are the experimentally set pressure, power, and flow rates, and in each case, the concentrations of various species, electron properties (density and temperature), ion temperature, gas temperature, and substrate temperature were computed. Plasma processes contain numerous species (ions and neutrals) participating in a large number of reactions, and it is not feasible to consider all of them in multidimensional simulations. The species included in the present model were chosen by first using a simpler 0-D volume averaged code[27] with over 100 species and almost 900 reactions for the NH_3/C_2H_2 feedgas. Extremely slow reactions and trace species were eliminated, and the remaining set includes 20 neutral species (NH_3, NH_2, NH, N_2, N, H_2, H, C_2H_4, C_2H_3, C_2H_2, C_2H, C_2, CH_4, CH_3, CH_2, CH, C, HCN, CN, HC_3N), 4 charged species (NH_3^+, NH_2^+, $C_2H_2^+$, e^-), and 175 reactions. The reaction set includes electron impact dissociation and ionization reactions, charge exchange reactions, electron−ion recombination, gas-phase radical exchange and dissociation reactions, and three-body recombination reactions.

Figure 3a displays the cathode temperature from experimental measurements and simulation as a function of plasma power, with C_2H_2 and NH_3 flow rates held constant. Here, the external tungsten heater is turned off. As the power is increased from 20 to 200 W, the plasma voltage rose from 595 to 683 V. A stronger increase in plasma current (34−294 mA) was observed due to an increasing plasma density with power. Even at a low power of 20 W, the cathode reached temperatures as high as 200−250 °C. Two pressure conditions (i.e., 5 mbar and 12 mbar) are shown in Figure 3a, and the temperature vs power curves are virtually identical. This indicates that the input power is the key parameter in determining the equilibrium cathode temperature

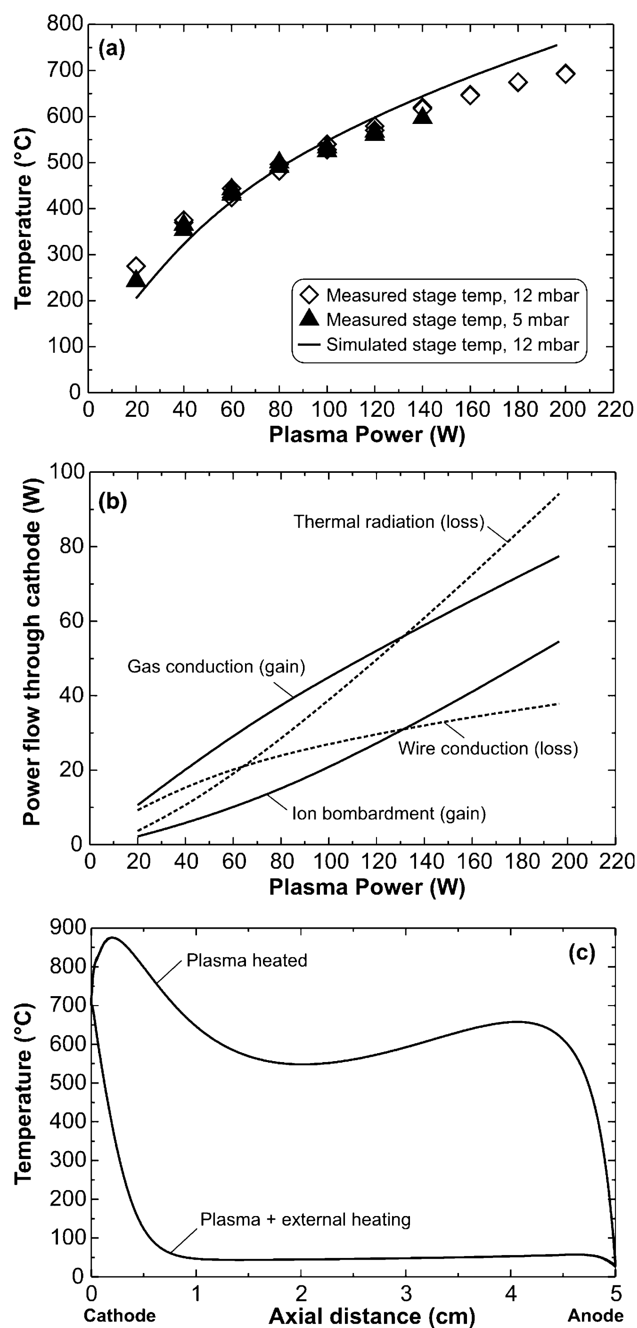

Figure 3. (a) Measured and simulated cathode temperatures as a function of plasma power. The gas mixture simulated was 54:200 sccm C_2H_2/NH_3 at 12 mbar. (b) Simulated power flows through the cathode under the same conditions. The dashed line denotes mechanisms in which energy is gained in the cathode (i.e., heating), and solid lines denote energy loss mechanisms (i.e., cooling). The total power through the cathode varies between 64 and 67% of the total input plasma power. (c) Cathode-to-anode temperature profiles for the cases of pure plasma heating vs plasma plus external heating.

in this pressure range. The comparison between the simulation and the experimental measurements is quite good for the entire range of powers examined. The slight disagreement at low and high powers is in part due to the assumption of a constant platform heat transfer coefficient in the model. Additional error results from the contact resistance of the thermocouple, which would result in an experimental underestimate of temperature. This error is estimated to be only

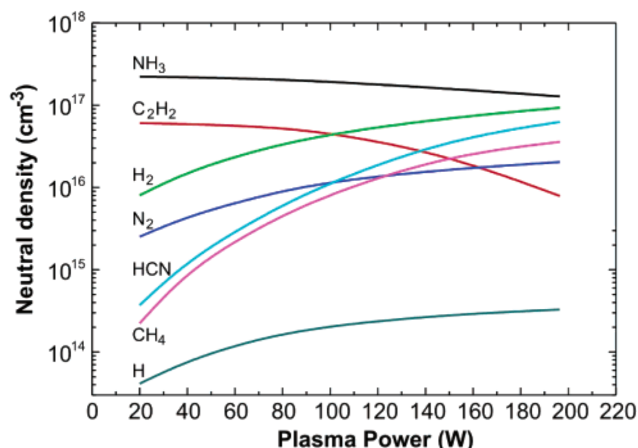

Figure 4. Simulated neutral species in the gas phase as a function of plasma power. The six most dominant species with atomic hydrogen are shown here.

1.7% by comparing an expected thermal contact resistance with the axial heat conduction by the thermocouple. However, the assumptions in this estimate are significant, having neglected the heating and cooling mechanisms at the thermocouple surface. A more detailed examination would be necessary to precisely quantify this error magnitude.

Figure 3b shows how the substrate platform power balance from eq 2 varies with plasma power. For the 12 mbar pressure considered, gas conduction is the primary mechanism for substrate heating. As power is increased, the relative importance of ion bombardment increases but never exceeds gas conduction. The high pressure results in a fairly collisional plasma such that significant heating of the gas occurs, and as such the hot gas is the main source for substrate heating. In contrast, at lower pressure (5 mbar, not shown here), the plasma is less collisional, less of the power is transferred to the gas, and thus ion bombardment surpasses gas conduction as the primary source of substrate heating at higher power. With regards to energy exiting the platform, the loss is dominated by thermal radiation for a significant portion of the power range. Thermal conduction does play a role at lower values of power ($<$65 W), but since the cathode is essentially thermally isolated, its role is secondary for the power range of interest for growth.

In Figure 3c, we compare the simulated gas temperature profiles arising from a plasma plus tungsten heater process and from pure plasma heating only, corresponding to the pictures in Figure 1a and b, respectively. In both cases, the substrate temperature in the simulation is fixed at 700 °C as is achieved in the experiments by adjusting the dc power to the cathode and power to the resistive tungsten heater. When plasma heating is the only source (with 200 W dc power and external heater off), the gas reaches high temperatures throughout the volume and peaks at 880 °C near the edge of the cathode sheath. It is clear that this hot gas heats the cathode. In the case of plasma plus external heater, the plasma power to the cathode is relatively low at 66 W since additional heating is provided by the resistive heater to obtain the same 700 °C. As expected, the gas temperature drops off rapidly away from the substrate.

Figure 4 shows the number densities of the six most abundant species and atomic hydrogen as a function of plasma power without an external heater. Acetylene dissociates more than ammonia at all power levels. The hydrogen abstraction reaction is a key source of radical and H_2 production. The atomic hydrogen production increases with plasma power, and this is likely to affect the morphology of the nanostructures. Figure 5 shows magnified SEM images at various conditions. The morphology in Figure 5a, corresponding to conditions in Figure 2c, is of nanostructures that are slightly undercut. As this case uses 200 W of plasma power with no external heater, the atomic hydrogen density is high, which may lead to undesirable etching of the nanofibers. Altering the conditions to reduce the H concentration should remove this effect, which is demonstrated in Figure 5b by adjusting the feedstock to 54:132 sccm C_2H_2/NH_3, effectively reducing the NH_3/C_2H_2 ratio. Figure 5c provides a magnified image of the nanostructures in Figure 2d; here, the combined heating (66 W plasma and the resistive heater on) yields nanofibers twice as tall as those from the plasma-only heating case. The density profiles in Figure 4 indicate that at 66 W there is more acetylene than at 200 W, while the reverse is true for methane. As acetylene dissociates on the Ni catalyst more readily than does methane,[28] the observed higher growth rate in Figure 2d

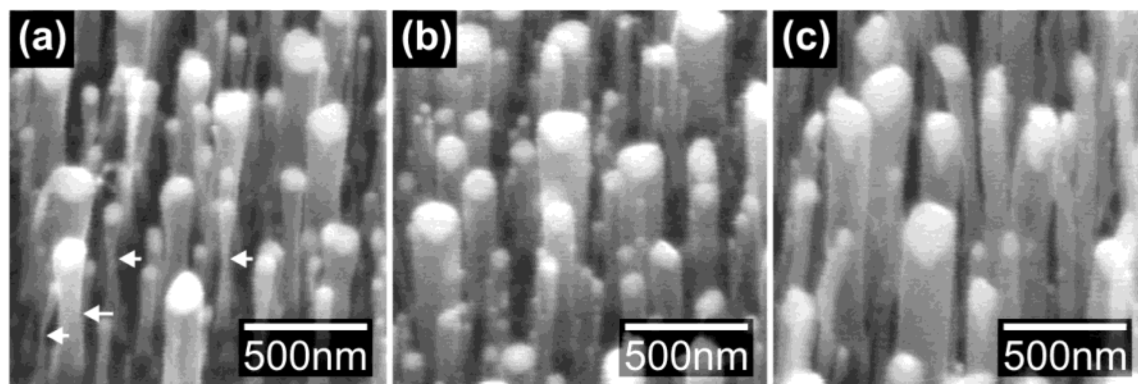

Figure 5. High magnification views of the nanofibers obtained from: (a) 200 W plasma power, 54:200 sccm C_2H_2/NH_3, 12 mbar, 700 °C, 15 min; the arrows show undercutting of the nanofibers as is described in the text; (b) 200 W plasma power, 54:132 sccm C_2H_2/NH_3, 12 mbar, 700 °C, 15 min; and (c) 66 W plasma power, 250 W heater power, 54:200 sccm C_2H_2:NH_3, 12 mbar, 700 °C, 15 min. The tilt was 45°.

compared to 2c is consistent. Last, the high degree of alignment of nanofibers from our plasma-heated process is a result of the high sheath electric field (simulated to be 0.5 V/μm) resulting from the high dc bias at the cathode where the sample is placed, in contrast with the curly structures obtained from the low applied dc or self-bias fields in refs 16−19.

In summary, we have shown that a substrate exposed to the plasma in a simple, parallel plate dc PECVD reactor for nanotube growth heats to high temperatures (~700 °C) without the aid of an external heater. This was used to synthesize straight and well-aligned carbon nanofibers. Simulation of the PECVD process has provided an understanding of the various mechanisms leading to the substrate heating and also explains the key differences in the structures of the nanotubes obtained from plasma heating. The substrate temperatures at various levels from measurement and simulations are in good agreement. Though this work is limited to only dc discharges; similar conclusions are expected for rf, inductive, and microwave reactors. Indeed, both experimental diagnostics[29−33] and modeling[31,34−37] of gas and substrate heating in inductive and electron cyclotron resonance plasmas used in semiconductor processing have been reported. All of this suggests that a deliberate cooling of the substrate needs to be introduced if room temperature or low-temperature growth is desired for a given set of conditions, including a reasonable power.

From a reactor design point of view, while plasma heating may obviate the need for an external heater, addition of the latter provides a higher level of process control and flexibility as the plasma can then be varied independent of the substrate temperature. The role of the applied power or dc bias is not only to heat the substrate but also to generate reactive species, through sustaining the plasma. Desired high temperatures can be obtained through a combination of low applied bias and external heating, whereas desired low temperatures can be reached by any combination of bias and cooling. This flexibility is also important in remote plasma operations where the reactive species are extracted from the plasma zone and used downstream where the growth occurs. As much as growth at low or room temperature is desirable for the flexibility to use glass, plastic, and other flexible but heat-susceptible substrates, it is not clear if nanofiber material quality can still be maintained, and this deserves further research.

Acknowledgment. K.B.K.T. acknowledges the support of Christ's College, Cambridge. B.A.C is supported by the University Affiliated Research Center (UARC) at NASA Ames, operated by the University of California at Santa Cruz under contract NAS2-031434. D.B. is with ELORET Corporation, and his work is supported by a subcontract from UARC. Discussions with Alan Cassell are acknowledged.

References

(1) Delzeit, L.; McAninch, I.; Cruden, B. A.; Hash, D.; Chen, B.; Han, J.; Meyyappan, M. *J. Appl. Phys.* **2002**, *91*, 6027.
(2) Ren, Z. F.; Huang, Z. P.; Xu, J. W.; Wang, J. H.; Bush, P.; Siegal, M. P.; Provencio, P. N. *Science* **1998**, *282*, 1105.
(3) Merkulov, V. I.; Lowndes, D. H.; Wei, Y. Y.; Eres, G.; Voelkl, E. *Appl. Phys. Lett.* **2000**, *76*, 3555.
(4) Chhowalla, M.; Teo, K. B. K.; Ducati, C.; Rupesinghe, N. L.; Amaratunga, G. A. J.; Ferrari, A. C.; Roy, D.; Robertson, J.; Milne, W. I. *J. Appl. Phys.* **2001**, *90*, 5308.
(5) Guillorn, M. A.; Melechko, A. V.; Merkulov, V. I.; Hensley, D. K.; Simpson, M. L.; Lowndes, D. H. *Appl. Phys. Lett.* **2002**, *81*, 3660.
(6) Koehne, J.; Chen, H.; Li, J.; Cassell, A. M.; Ye, Q.; Ng, H. T.; Han, J.; Meyyappan, M. *Nanotechnolology* **2003**, *14*, 1239.
(7) Zhang, L.; Melechko, A. V.; Merkulov, V. I.; Guillorn, M. A.; Simpson, M. L.; Lowndes, D. H.; Doktycz, M. J. *Appl. Phys. Lett.* **2002**, *81*, 135.
(8) Lau, K. K. S.; Bico, J.; Teo, K. B. K.; Chhowalla, M.; Amaratunga, G. A. J.; Milne, W. I.; McKinley, G. H.; Gleason, K. K. *Nano Lett.* **2003**, *3*, 1701.
(9) Kato, T.; Jeong, G.-H.; Hirata, T.; Hatakeyama, R.; Tohji, K.; Motomiya, K. *Chem. Phys. Lett.* **2003**, *381*, 422.
(10) Bower, C.; Zhu, W.; Jin, S.; Zhou, O. *Appl. Phys. Lett.* **2000**, *77*, 830.
(11) Caughman, J. B. O.; Baylor, L. R.; Guillorn, M. A.; Merkulov, V. I.; Lowndes, D. H.; Allard, L. F. *Appl. Phys. Lett.* **2003**, *83*, 1207.
(12) Meyyappan, M.; Delzeit, L.; Cassell, A.; Hash, D. *Plasma Sources Sci. Technol.* **2003**, *12*, 205.
(13) Han, J.-H.; Yang, W.-S.; Yoo, J.-B.; Park, C.-Y. *J. Appl. Phys.* **2000**, *88*, 7363.
(14) Hayashi, Y.; Negishi, T.; Nishino, S. *J. Vac. Sci. Technol. A* **2001**, *19*, 1796.
(15) Cruden, B. A.; Cassell, A. M.; Ye, Q.; Meyyappan, M. *J. App. Phys.* **2003**, *94*, 4070.
(16) Choi, Y. C.; Bae, D. J.; Lee, Y. H.; Lee, B. S.; Park, G. S.; Choi, W. B.; Lee, N. S.; Kim, J. M. *J. Vac. Sci. Technol. A* **2000**, *18*, 1864.
(17) Okai, M.; Muneyoshi, T.; Yaguchi, T.; Sasaki, S. *Appl. Phys. Lett.* **2000**, *77*, 3468.
(18) Wilson, J. I. B.; Scheerbaum, N.; Karim, S.; Polwart, N.; John, P.; Fan, Y.; Fitzgerald, A. G. *Diamond Relat. Mater.* **2002**, *11*, 918.
(19) Boskovic, B. O.; Stolojan, V.; Khan, R. U. A.; Haq, S.; Silva, S. R. P. *Nature Materials* **2002**, *1*, 165.
(20) Hofmann, S.; Ducati, C.; Robertson, J.; Kleinsorge, B. *Appl. Phys. Lett.* **2003**, *83*, 135.
(21) Teo, K. B. K.; Lee, S.-B.; Chhowalla, M.; Semet, V.; Binh, V. T.; Groening, O.; Castignolles, M.; Loiseau, A.; Pirio, G.; Legagneux, P.; Pribat, D.; Hasko, D. G.; Ahmed, H.; Amaratunga, G. A. J.; Milne, W. I. *Nanotechnology* **2003**, *14*, 204.
(22) Teo, K. B. K.; Chhowalla, M.; Amaratunga, G. A. J.; Milne, W. I.; Hasko, D. G.; Pirio, G.; Legagneux, P.; Wyczisk, F.; Pribat, D. *Appl. Phys. Lett.* **2001**, *79*, 1534.
(23) Hash, D.; Bose, D.; Govindan, T. R.; Meyyappan, M. *J. Appl. Phys.* **2003**, *93*, 6284.
(24) Bose, D.; Govindan, T. R.; Meyyappan, M. *J. Electrochem. Soc.* **1999**, *146*, 2795.
(25) Winters, H. F.; Coufal, H.; Rettner, C. T.; Bethune, D. S. *Phys. Rev. B* **1990**, *41*, 6240.
(26) Leroy, O.; Perrin, J.; Jolly, J.; Péalat, M.; Lefebvre, M. *J. Phys. D: Appl. Phys.* **1997**, *30*, 499.
(27) Hash, D.; Meyyappan, M. *J. Appl. Phys.* **2003**, *93*, 750.
(28) Baker, R. T. K.; Harris, P. S. In *Chemistry and Physics of Carbon*; Walker, P. L., Jr., Thrower, P. A., Eds.; Dekker: New York, 1978; Vol. 14, p 83.
(29) Hebner, G. A. *J. Appl. Phys.* **1996**, *80*, 2624.
(30) Malyshev, M. V.; Donnelly, V. M.; Downey, S. W.; Colonell, J. I.; Layadi, N. *J. Vac. Sci. Technol. A* **2000**, *18*, 849.
(31) Kiehlbauch, M. W.; Graves, D. B. *J. Appl. Phys.* **2001**, *89*, 2047.
(32) Abada, H.; Chabert, P.; Booth, J. P.; Robiche, J.; Cartry, G. *J. Appl. Phys.* **2002**, *92*, 4223.
(33) Tonnis, E. J.; Graves, D. B. *J. Vac. Sci. Technol. A* **2002**, *20*, 1787.
(34) Bukowski, J. D.; Graves, D. B.; Vitello, P. *J. Appl. Phys.* **1996**, *80*, 2614.
(35) Nam, S. K.; Shin, C. H.; Economou, D. J. *Mater. Sci. Semicond. Process.* **1999**, *2*, 271.
(36) Bogaerts, A.; Gijbels, R.; Serikov, V. V. *J. Appl. Phys.* **2000**, *87*, 8334.
(37) Hash, D. B.; Bose, D.; Rao, M. V. V. S.; Cruden, B. A.; Meyyappan, M.; Sharma, S. P. *J. Appl. Phys.* **2001**, *90*, 2148.

NL049629G